A Mode-switching Strategy of Droop Control for VSC-MTDC Systems Considering Maximum DC Voltage Regulation Capability

Yizhen Wang, *Member*, *IEEE*, Fengliang Qiu, Zhongguan Wang, *Member*, *IEEE*, Yirun Ji, Zhengguang Chen, and Chengshan Wang, *Senior Member*, *IEEE*

***Abstract*—To achieve the goal of carbon neutrality, renewable energy integration through a voltage source converter based multi-terminal direct current (VSC-MTDC) system has been identified as a promising solution. To tackle the significant DC voltage over-limit problem in a VSC-MTDC system during disturbances, this paper proposes a mode-switching strategy of droop control considering maximum DC voltage regulation capability. The close relationship between node injection powers and node DC voltages in the MTDC system is elaborated, and the most effective regulation approach of local injection power for limiting DC voltage deviation is presented. The operating point trajectories of different droop control explains that the DC voltage deviation can be minimized by fully utilizing the capacity of converters. Therefore, the mode-switching strategy with the maximum DC voltage regulation capability is realized by the switching between the voltage droop control and the constant maximum power control. In addition, a mode recovery process and a smooth switching method are developed to make converters regain the capability of maintaining DC voltage and reduce power fluctuation during mode switching, respectively. Furthermore, three cases are investigated to verify the effectiveness of the proposed mode-switching strategy. Compared with simulation results of the conventional droop control and the DC voltage deviation-dependent droop control, better performance of transient and steady-state DC voltage deviation is achieved through the proposed strategy.**

***Index Terms*—Droop control, maximum DC voltage regulation capability, mode-switching, VSC-MTDC.**

I. Introduction

ENVIRONMENT protection and renewable energy integration have been urgent issues that are widely discussed around the world. Providing affordable, reliable, and modern energy services and increasing the share of sustainable energy in the global energy mix are contained in seventeen goals of the *2030 Agenda for Sustainable Development* proposed by the United Nations [1]. China has promised to reach the carbon emission peak around 2030 and achieve carbon neutrality by 2060 [2]. For these goals, it is imperative to build a secure, clean, and smart power system with a renewable energy priority. It has been proved that the direct current (DC) system plays an important role in integrating renewable energy and stabilizing energy fluctuation, which has a promising prospect in reducing carbon emissions [3]–[5].

Compared with line commutated converters (LCC), voltage source converters (VSC) possess various advantages [6], such as high electricity quality, no commutation failure, decoupled and fast control of active and reactive power, and bidirectional power flow without DC polarity reversal. Consequently, a VSC based multi-terminal direct current (VSC-MTDC) system has been a suitable and effective solution for large-scale renewable energy integration, such as offshore wind farms.

Many studies have focused on VSC-MTDC, including AC/DC hybrid power flow algorithms [7], [8], system modeling and stability analysis [9], [10], system dispatch and hierarchical control [11], etc. In addition, frequency support through MTDC has been wildly investigated, nevertheless, which is more suitable in multi-area interconnection and wide-area DC grids than renewable energy integration due to its intermittence [12], [13]. Moreover, since the DC voltage is an indicator related to the DC system stability, the problem of serious DC voltage over-limit caused by output power fluctuation of renewable energy or faults, such as converter outage needs to be further researched.

Both the master-slave (M-S) method and voltage droop control method (VDM) belong to system voltage control schemes, which are applied commonly in VSC-MTDC systems [14]. Features of the M-S method can be summarized as simplicity, accuracy, but unreliability, since only one VSC regulates the DC voltage and undertakes all the imbalanced power while the others operate in the constant power control mode. By contrast, as one of the decentralized methods, the VDM can enhance the reliability of MTDC systems since every droop-controlled converter simultaneously share the imbalanced power burden. Meanwhile, the application of VDM also leads to complicated control mechanisms and considerable DC voltage deviations during large disturbances.

In order to regulate the DC voltage within the safety limit, a novel adaptive droop coefficient method is proposed in [15], which considers the local DC voltage deviation and the loading

Manuscript received July 16, 2021; revised October 11, 2021; accepted December 9, 2021. Date of online publication August 18, 2022; date of current version April 22, 2024. This work was supported in part by the National Natural Science Foundation of China under Grant 52377119 and U22B20109.

Y. Z. Wang, F. L. Qiu, Z. G. Wang (corresponding author, email: wang_zg@tju.edu.cn), and C. S. Wang are with Key Laboratory of Smart Grid of Ministry of Education, Tianjin University, Tianjin 300072, China.

Y. R. Ji is with Electric Power Research Institute of State Grid JiBei Electric Power Co. Ltd., Beijing 100045, China.

Z. G. Chen is with State Grid Corporation of China, Beijing 100031, China.

DOI: 10.17775/CSEEJPES.2021.05150

factor. Converters that possess smaller DC voltage deviation or bigger power headroom will undertake more imbalanced power. Further research on adaptive control schemes have been studied in [16], in which the droop gain perturbation technique is proposed. Based on the global and local loading factor and available headroom of converters, the modified adaptive droop control approaches are investigated. Likewise, [17] presents a nonlinear design methodology of droop control to achieve the same target in DC microgrids. Combined with stability criterion, [18] has developed a coordinated method to determine droop coefficients aimed at avoiding overload and achieving better DC voltage deviation and transient variation. [19] changes the droop coefficient based on the frequency consensus and the optimization considering power losses, generation cost, and frequency deviation cost. In addition, an optimal algorithm and power flow control are achieved in [20], which changes the setpoint of VDM to minimize the transmission losses in meshed AC/DC grids and the DC voltage deviation in a MTDC system at the same time. [21] presents an improved droop controller for regulating the DC voltage close to its reference, which requires communication with the neighboring converter.

Nowadays, the research on VDM primarily focuses on adaptive droop control methods and system optimal control methods with fast communication required. These approaches either alter system parameters or spend a relatively long calculation time so that converters cannot participate in transient regulation in time. However, improper parameters affect system stability [22]. Insufficient DC voltage regulation capability also reduces DC voltage stability. Furthermore, since the output power of renewable energy has intrinsic intermittence and fluctuation, it is difficult to reach a steady-state for the adaptive droop method which will continuously change the droop gain over the entire range of DC voltage deviations. With these in mind, a novel strategy is developed to tackle the DC voltage deviation problem before the centralized control implement.

This paper proposes a mode-switching strategy of droop control for VSC-MTDC systems, and the main contributions of this paper are summarized as follows.

1) The mode-switching strategy makes full use of the maximum capacity of droop-controlled converters to limit DC voltage deviations. The relationship between the node injection power and the node DC voltage is analyzed, which proves that the proposed strategy has the largest capability for DC voltage regulation.

2) The local DC voltage is limited within the specified range by smooth mode switching between the voltage droop control and the constant maximum power control.

3) The existing control modes of VSCs are retained and the system stability is not affected by the mode-switching strategy since controller parameters and droop coefficients are not modified. In addition, the communication condition is not required.

The remainder of this paper is structured as follows. In Section II, the influence of the MTDC system injection power on the DC voltage deviation is described, the mechanism of the VDM is simply introduced, and the mathematical relationship between the node injection power and node DC voltage is revealed. Section III proposes the mode-switching strategy and elaborates its procedures in detail. Three simulation cases are investigated to validate the mode-switching strategy in Section IV. Finally, the conclusion is presented in Section V.

II. Relationship Between Power and DC Voltage

A. Equivalent Capacitance Model of the MTDC System

The topology diagrams of the two-level VSC, the modular multilevel converter (MMC) and its half-bridge submodule are depicted in Fig. 1, both consist of a DC-link capacitor. Likewise, so do LCCs and DC-DC converters, such as buck-boost. Thus, , each converter station of the MTDC system contains at least one DC-link capacitor [23], [24]. The composition of these DC-link capacitors resists DC voltage deviation under imbalanced power in nature. In addition, the DC voltage changing rate of the MTDC system is also affected by these capacitors.

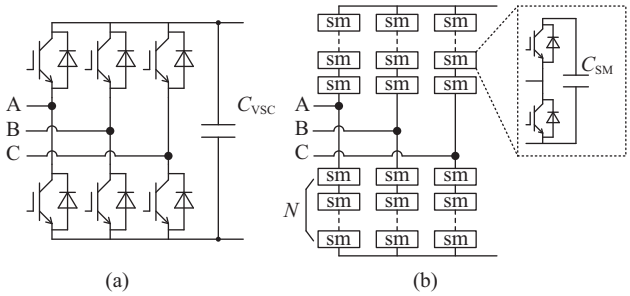

Fig. 1. Topology structure diagram of (a) a two-level VSC and (b) an MMC and its half-bridge submodule.

For simplicity and clarity, the per-unit system is adopted in this paper. As depicted in Fig. 2, after ignoring the transmission line resistance and inductance, the entire MTDC system can be considered as an equivalent system capacitance with an input port and an output port. The equivalent system capacitance $C_{\rm sys}$ is composed of the capacitance of each converter and the distributed capacitance of transmission lines or cables. Under this assumption, the DC voltages of each node of the MTDC system are identical to the DC voltage $V_{\rm dc}$. Thus, the relationship between the DC current and DC voltage can be described as:

$$\sum_{k=1}^{m} I_{k\rm in} - \sum_{k=m+1}^{n} I_{k\rm out} = C_{\rm sys}\frac{{\rm d}V_{\rm dc}}{{\rm d}t} \tag{1}$$

where $I_{k\rm in}$ and $I_{k\rm out}$ represent the current injects into and which absorbs from the MTDC system by the kth converter, respectively. Converters numbered 1 to m are in rectifier and converters numbered $m+1$ to n are in inverter. $C_{\rm sys}$ represents the system capacitance and $V_{\rm dc}$ represents the DC voltage.

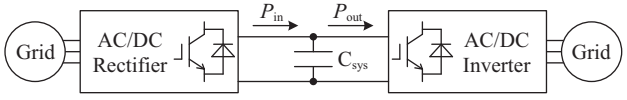

Fig. 2. The ideal equivalent circuit of the MTDC system.

By multiplying $V_{\rm dc}$ at both sides, (1) can be transformed to:

$$P_{\rm in} - P_{\rm out} = C_{\rm sys}\frac{{\rm d}V_{\rm dc}}{{\rm d}t}V_{\rm dc} \tag{2}$$

where $P_{\rm in}$ and $P_{\rm out}$ denote the injection power and absorption power, respectively.

Usually, the DC voltage of the MTDC system is restricted within a very small range near the rated DC voltage, which can be regarded as the base voltage value of the per-unit system, so$V_{\rm dc} \approx$1, and (2) can be expressed by:

$$P_{\rm in} - P_{\rm out} = C_{\rm sys}\frac{{\rm d}V_{\rm dc}}{{\rm d}t} \tag{3}$$

From (3), the DC voltage deviation can be eliminated if an appropriate power regulation has been implemented.

B. Voltage Droop Control Method

The voltage droop control has been widely discussed since its high reliability, which is also an applicative and promising solution in control schemes for the MTDC system. The voltage droop control is a combination of constant active power control and constant DC voltage control, nevertheless, it is a tradeoff between power flow redistribution and DC voltage regulation. It is defined that the power injects into the DC system is positive. The characteristic curve and the control block diagram of the voltage droop control are depicted in Fig. 3 and the control law of it can be expressed as:

$$(P - P_{\rm ref}) + \beta(V_{\rm dc} - V_{\rm dcref}) = 0 \tag{4}$$

where P and $P_{\rm ref}$ denote the active power and its reference to the converter, respectively. $V_{\rm dcref}$ represents the reference DC voltage and β represents the droop gain. In addition, $V_{\rm dc} - V_{\rm dcref}$ is defined as DC voltage deviation $\Delta V_{\rm dc}$.

C. Influence of Node Injection Power on Node DC Voltage

The linear power flow algorithm proposed in [25] provides an accurate and fast method to acquire the steady-state of the MTDC system. Supposing there are n nodes in a MTDC system, the generalized power-flow model including the droop characteristic can be expressed as:

$$\underbrace{\boldsymbol{P}_{\rm ref} = \boldsymbol{A}\Delta\boldsymbol{V}_{\rm dc}}_{\text{linear equation}} + \underbrace{{\rm o}^2(\Delta\boldsymbol{V}_{\rm dc})}_{\text{neglect}} \tag{5}$$

$$\boldsymbol{P}_{\rm ref} = [P_{1{\rm ref}} \quad P_{2{\rm ref}} \quad \cdots \quad P_{n{\rm ref}}]^{\rm T} \tag{6}$$

$$\boldsymbol{A} = \begin{bmatrix} Y_{1,1}+\beta_1 & Y_{1,2} & \cdots & Y_{1,n} \\ Y_{2,1} & Y_{2,2}+\beta_2 & \cdots & Y_{2,n} \\ \vdots & \vdots & \ddots & \vdots \\ Y_{n,1} & Y_{n,2} & \cdots & Y_{n,n}+\beta_n \end{bmatrix} \tag{7}$$

$$\Delta\boldsymbol{V}_{\rm dc} = [\Delta V_{1{\rm dc}} \quad \Delta V_{2{\rm dc}} \quad \cdots \quad \Delta V_{n{\rm dc}}]^{\rm T} \tag{8}$$

where $\boldsymbol{Y}$ is the element in the system admittance matrix, and $\Delta\boldsymbol{V}_{\rm dc}$ is the DC voltage error vector. Subscripts 1 to n denote the DC node number.

An extra virtual node is generated by using the generalized power-flow model. As illustrated in [26], the virtual node in the MTDC system is a constant DC voltage node numbered $n+1$, which is connected to every DC node by admittance β.

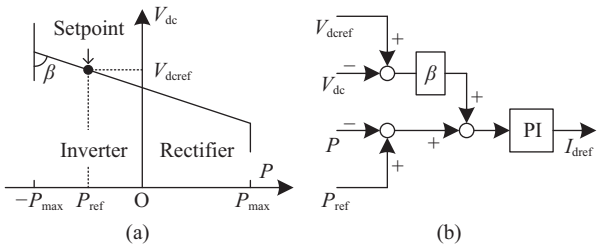

Fig. 3. (a) P-V characteristic curve and (b) controller block diagram of VDM.

To investigate the node injection power and node DC voltage, equation (5) is treated as follows.

$$\frac{\partial\boldsymbol{P}_{\rm ref}}{\partial\boldsymbol{P}_{\rm ref}^{\rm T}} = \frac{\partial\boldsymbol{A}\Delta\boldsymbol{V}_{\rm dc}}{\partial\boldsymbol{P}_{\rm ref}^{\rm T}} \tag{9}$$

$$\boldsymbol{A}^{-1} = \begin{bmatrix} \frac{\partial\Delta V_{1{\rm dc}}}{\partial P_{1{\rm ref}}} & \frac{\partial\Delta V_{1{\rm dc}}}{\partial P_{2{\rm ref}}} & \cdots & \frac{\partial\Delta V_{1{\rm dc}}}{\partial P_{n{\rm ref}}} \\ \frac{\partial\Delta V_{2{\rm dc}}}{\partial P_{1{\rm ref}}} & \frac{\partial\Delta V_{2{\rm dc}}}{\partial P_{2{\rm ref}}} & \cdots & \frac{\partial\Delta V_{2{\rm dc}}}{\partial P_{n{\rm ref}}} \\ \vdots & \vdots & \ddots & \vdots \\ \frac{\partial\Delta V_{n{\rm dc}}}{\partial P_{1{\rm ref}}} & \frac{\partial\Delta V_{n{\rm dc}}}{\partial P_{2{\rm ref}}} & \cdots & \frac{\partial\Delta V_{n{\rm dc}}}{\partial P_{n{\rm ref}}} \end{bmatrix} \tag{10}$$

Matrix $\boldsymbol{A}^{-1}$ is the inverse of $\boldsymbol{A}$, meanwhile, it is a special node impedance matrix. Because $\boldsymbol{A}$ is constituted by admittance and droop gain, every element in $\boldsymbol{A}^{-1}$ is positive. Consistent with the above, the DC voltage is positively correlated with the injection power, for example, all node DC voltages rise with arbitrary node injection power increasing. Furthermore, $\boldsymbol{A}$ is a diagonal dominance matrix with the main diagonal element of self-impedance. Consequently, once the voltage of a node exceeds the specified range, regulating its own injection power will maximize the improvement of the DC voltage condition.

III. Mode-Switching Strategy

The mode-switching strategy is proposed based on the discussion on the relationship between injection power and DC voltage, which restricts the DC voltage deviation through local injection power regulation. The flow chart diagram of the mode-switching strategy is illustrated in Fig. 4.

A. Trigger and Mode Switching

The trigger threshold voltage $\delta_{\rm tri}$ of each converter should be set in advance, which acts as a trigger for mode switching. When the node DC voltage reaches the threshold value, the operation mode of the converter immediately switches from the voltage droop control to the constant maximum power control to alleviate DC voltage deviations. The direction of reference power in constant power control should be determined based on the direction of DC voltage deviation [27], so $P_{\rm ref}$ is equal to $\mathrm{sgn}(-\Delta V_{\rm dc})P_{\rm max}$ accordingly, where sgn denotes signum and $P_{\rm max}$ represents the maximum power of a converter.

The proposed strategy considers the maximum DC voltage regulation capacity, and its explanation is illustrated in Fig. 5. Located on the voltage droop control plane, the trajectory of the conventional VDM operating point as the voltage decreases is marked with a red solid line in Fig. 5. The injection energy is the integral of its power over time, which is the shadow marked

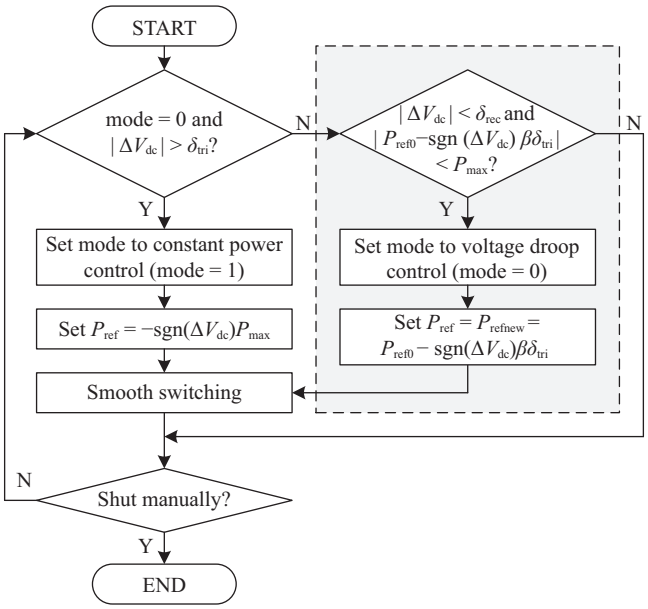

Fig. 4. Flow chart of the mode-switching strategy.

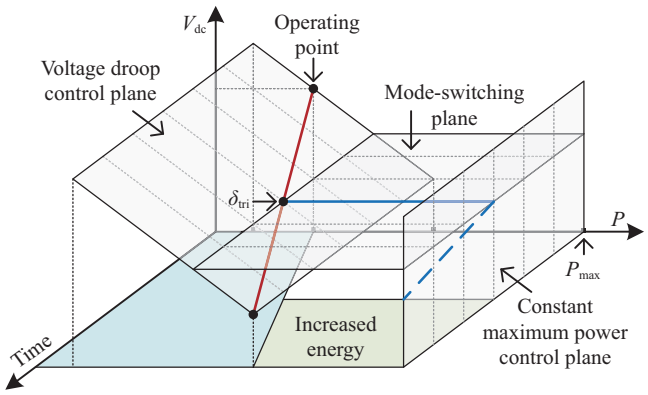

Fig. 5. P-V planes and time-varying trajectories of the operating point under conventional voltage droop control and mode-switching strategy.

in blue. With the mode-switching strategy, the operating point will cross the mode-switching plane to the constant maximum power control plane when the DC voltage reaches the trigger threshold. The blue line in Fig. 5 denotes the trajectory of the mode-switching strategy operating point, where the dotted line indicates a possible trajectory under constant maximum power control. The increased energy injected by the proposed strategy is marked in green, its area is greater than that of any method to change droop coefficients at this trigger threshold. According to (3), the proposed strategy maximizes the increased energy, so it considers the maximum voltage regulation capacity.

The trigger threshold is always set below the DC voltage limit to provide voltage margin and avoid voltage excess, such as $\delta_{\mathrm{tri}} = 0.8\delta_{\mathrm{lim}}$, where δ_{lim} represents the safety limit. Meanwhile, the trigger threshold cannot be set too low, otherwise, the mode switching may be triggered frequently during system normal operations. When the trigger threshold voltages of all the droop-controlled converters are set the same, the converter stations close to the power source or load are easier to participate in mode switching due to their greater voltage deviation. Therefore, for better DC voltage regulation and power-sharing, a relatively low threshold should be set in converters with large capacities and strong AC systems.

It should be noted that once all droop-controlled converters participate in constant maximum power control, the maximum DC voltage regulation capability of the MTDC system is realized, and the increasing tendency of DC voltage deviation will be curbed faster than other methods. However, at the same time, the MTDC system voltage cannot be directly maintained by any converter and the DC voltage will continuously increase or decrease until a converter station switches back to voltage droop control mode.

B. Mode Recovery Process

The above analysis indicates that the DC voltage reliability decreases because the voltage droop control mode is switched to constant maximum power control. Thus, when DC voltage is restored to a reasonable range after the transient process, that is, the DC voltage deviation is below the recovery voltage threshold δ_{rec}, it is necessary to switch the converter mode from constant maximum power control to voltage droop control. This part is the mode recovery, which makes droop-controlled converter stations regain the DC voltage control capability and maintain system voltages within a specified range at post-disturbance. However, converters with a high voltage deviation level will still operate under constant maximum power control.

In addition, in order to restrict DC voltage and power fluctuation, a hysteresis comparison between mode switching and recovery should be set, which means $\delta_{\mathrm{rec}} < \delta_{\mathrm{tri}}$. Furthermore, to keep the DC voltage around the nominal value and increase the voltage margin for the next disturbance, the reference power of VDM should be revised during mode recovery.

The imbalanced power cannot be exactly calculated only by using local information, whereas it determines the DC voltage deviation in the droop-controlled MTDC system through (5). When the DC voltage of a converter station just reaches the trigger threshold voltage, the DC voltage deviation will probably continue to broaden. Thus, when the kth converter activates the mode-switching, the imbalanced power is mostly greater than $\beta_k\delta_{\mathrm{tri}}$. Despite the DC voltage in transient being higher than that at the steady-state due to the dynamic process at post-disturbance, the system overshoot is not particularly high. Consequently, the new power reference can be expressed as:

$$P_{\mathrm{refnew}} = P_{\mathrm{ref0}} - \mathrm{sgn}(\Delta V_{\mathrm{dc}})\beta\delta_{\mathrm{tri}} \tag{11}$$

where P_{refnew} denotes the new reference power, P_{ref0} denotes the previous reference power of VDM, and $-\mathrm{sgn}(\Delta V_{\mathrm{dc}})\beta\delta_{\mathrm{tri}}$ is equal to the power shared by the converter that operates at its trigger threshold voltage at the steady-state.

In addition, the converter retains its mode (constant maximum power control) in case of $P_{\mathrm{refnew}} > P_{\mathrm{max}}$. Provided that the DC voltage triggers the mode-switching strategy again because the previous reference power cannot make the DC voltage within the trigger threshold, the mode recovery process will be continued and the setpoint will be revised until the system is stable.

C. Smooth Switching Mechanism

Since the different proportional coefficients are contained in different PI controllers, the prompt switching of the controller will lead to a step in controller output. To avoid the transient power variation during the mode switching process, a smooth switching method is developed, which is described as:

1) When a controller receives a switching signal, the instant output value of it (controller to be switched off) will be stored and transmitted to the controller to be switched on.

2) The integrator in the PI controller to be switched on is assigned an initial value, which can be calculated by:

$$INT_{\mathrm{ini}} = PI_{\mathrm{out}} - K_{\mathrm{p}} PI_{\mathrm{in}} \tag{12}$$

where INT_{ini} denotes the initial value to be assigned and PI_{out} denotes the output of the controller to be switched off. K_{p} and PI_{in} represents the proportional coefficient and the input of the controller to be switched on, respectively.

The diagram of the mode-switching strategy containing the smooth switching method is depicted in Fig. 6, where mode1 and mode 0 represent the mode of constant maximum power control and voltage droop control, respectively.

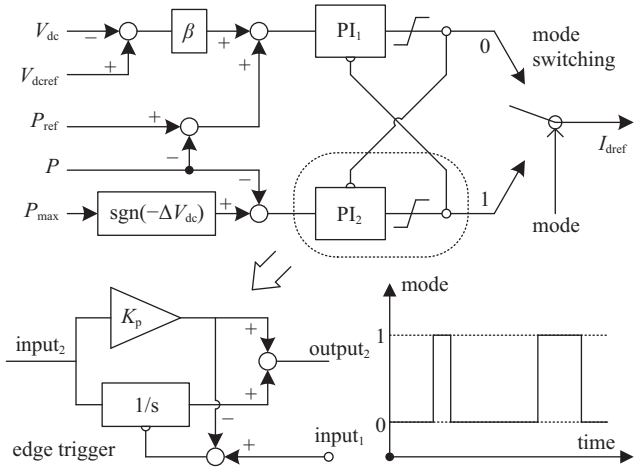

Fig. 6. Controller of the mode-switching strategy.

D. Discussion and Analysis

In fact, the mode-switching control strategy accelerates the proceedings of the voltage droop control, which shifts converter state from $|P| < 1$ to:

$$|P_{\mathrm{ref}} - \beta \Delta V_{\mathrm{dcc}}| = |P| = 1 \tag{13}$$

where ΔV_{dcc} represents the critical DC voltage for $|P| = 1$. In other words, the treatment of the high DC voltage deviation is utilized by the proposed strategy to tackle the situation of low DC voltage deviation.

Taking a four-terminal VSC-HVDC system as an example. The equivalent circuit diagram with four droop-controlled VSCs is shown in Fig. 7(a), where nodes N1 to N4 represent four DC buses connected with the VSC. Moreover, the diagram with VSC1 operating in constant maximum power control is shown in Fig. 7(b), which is the same as when the DC voltage deviation of VSC1 is equal to its critical DC voltage.

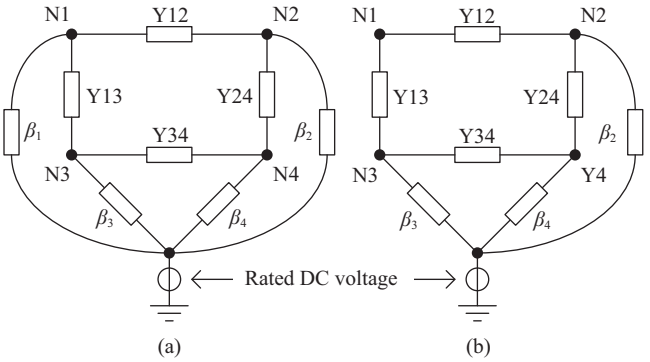

Fig. 7. Admittance diagram of a four-terminal HVDC system. (a) N1 to N4 are in VDM. (b) N1 is in constant power control and N2 to N4 are in VDM.

In addition, if the power of a converter station reaches its maximum when the DC voltage is greater than its trigger voltage, which means $|P_{\mathrm{ref}} - \mathrm{sgn}(\Delta V_{\mathrm{dc}})\beta\delta_{\mathrm{tri}}| > 1$, the necessity of mode-switching will be lost.

The combination between the voltage droop control and the constant maximum power control, and the smooth switching between them are achieved by the mode-switching strategy. It indicates that the existing controllers are retained, and only the mode-switching coordinated scheme needs to be added. Thus, the complexation of parameters tuning and the requirement for communication are avoided, in addition, system stability and system stiffness are preserved. According to Fig. 5, Fig. 7 and the relationship between injection power and DC voltage, it is certain that the proposed strategy fully mobilizes the converter to participate in power regulation and exploits the capability of each converter to prevent an over-limit of the DC voltage.

IV. Simulations

Three cases are studied to verify the effectiveness of the mode-switching strategy using PSCAD/EMTDC. The first case consists of output power steps of wind farms and a sequential converter outage. It aims at validating the capability of the proposed strategy to restrict DC voltage deviation rising in the case of converter outage after a power disturbance. Based on the first case, the comparison between the mode-switching strategy and the DC voltage deviation-dependent droop control according to [26] is investigated in the second case. Moreover, the third case contains a line disconnection and a sequential power step, which aims at validating the capability under the situation of the power disturbance after the line fault.

A five-terminal meshed VSC-HVDC system shown in Fig. 8 is adopted, where two offshore wind farms are connected to three separate and strong AC systems. Detailed parameters of the system are listed in Table I.

A. Case I

The disturbances in Case I are as follows: 1) At 1.2 s, the output power of wind farm1 increases from 100 MW to 350 MW, and the output power of wind farm 2 increases from 260 MW to 500 MW. 2) At 2.2 s, the VSC1 outage (F1 in Fig. 8) occurs. The simulation results of the comparison

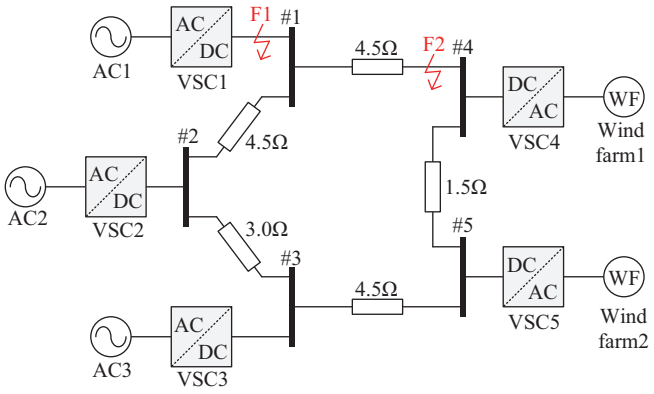

Fig. 8. Topology diagram of the five-terminal VSC-HVDC system.

TABLE I
PARAMETERS OF THE FIVE TERMINAL HVDC SYSTEM

Parameters	Value
Rated capacity/initial setpoint of VSC1	200/−60 MVA
Rated capacity/initial setpoint of VSC2	600/−180 MVA
Rated capacity/initial setpoint of VSC3	400/−120 MVA
Rated capacity/initial power of VSC4	600/100 MVA
Rated capacity/initial power of VSC5	600/260 MVA
Droop gains of droop-controlled VSCs	10.0 p.u.
System nominal DC voltage	± 200 kV
Safety limit of DC voltage deviation	5%
Trigger threshold of droop-controlled VSCs	4%
Recovery threshold of droop-controlled VSCs	2.5%
Proportional/time integral constant of inner current PI controller	0.6/0.01
Proportional/time integral constant of outer voltage droop PI controller	1.5/0.1
Proportional/time integral constant of outer constant power PI controller	0.2/0.05

between the proposed strategy and the conventional VDM are illustrated in Fig. 9. Both two disturbances lead to DC voltage rising because the injection power promptly increased.

With the conventional voltage droop control, it is obvious that the DC voltage of both VSC1 and VSC3 exceeds the safety limit during the first disturbance. During the next disturbance, the DC voltage of both VSC2 and VSC3 exceeds the safety limit. Furthermore, the steady-state DC voltage of VSC3 is beyond 420 kV. The setpoints and the droop gains among the droop-controlled converters remain unchanged, thus only the droop relationship between the power and the DC voltage contributes to the power dynamic performance. The DC voltage sensor is located between the VSC DC feeder and the DC breaker. So, when a VSC1 outage occurs and the DC breaker of VSC1 acts, the DC voltage of VSC1 will decrease.

With the mode-switching strategy, the DC voltages of VSC1, VSC2, and VSC3 are restricted and are within the specified range for all the time. Particularly, compared with the results from the conventional VDM, the peak DC voltage is reduced by 4 kV during the first disturbance, and 7 kV during the second disturbance by the proposed strategy. A relatively small steady-state DC voltage deviation is achieved by the proper setpoint regulation. As shown in Fig. 9, when the DC voltage of VSC1 reaches 416 kV at 1.280 s, the operation mode of VSC1 is switched to constant maximum power control. The mode of VSC3 is also switched to constant maximum power control at 1.294 s. However, since the DC voltage of VSC2 is below its trigger threshold value, it still operates in droop control mode. Next, after the trainset process, the DC voltage of VSC3 falls back below the recovery threshold 410 kV, thus the mode of VSC3 shifts from the constant maximum power control to the droop control. Meanwhile, the setpoint of VSC3 is changed from 0.3 p.u. to 0.7 p.u. according to (11). Due to the adoption of the smooth switching method, a smooth power dynamic process is observed when the setpoint is changed. In addition, when VSC1 reaches the recovery threshold, the same process is performed, and its setpoint is also changed to 0.7 p.u. Both VSC1 and VSC3 alleviate the DC voltage rising and reduce the DC voltage deviation at steady-state.

Subsequently, when the second disturbance (VSC1 outage) occurs, a similar treatment of converters is conducted. The DC voltage of VSC3 reaches its trigger threshold again at 2.251 s when the power of VSC3 is nearly its rated capacity. Thus, the effect of the mode-switching of VSC3 is of little significance at that time. Because its reference power is 1.1 p.u. in the next recovery process, the mode recovery will not be executed in VSC3. In other words, the operation mode of VSC3 remains at the constant maximum power control. On the contrary, the mode-switching and the mode-recovery are executed in VSC2, which alleviates the rising DC voltage. As shown in Fig. 9(b), the maximum power absorbed by VSC1 reaches 500 MW at 2.233 s. Then, it backs down to 403 MW at steady-state. The mode-switching conducted by VSC2 also contributes to the steady-state system DC voltage around its nominal value.

B. Case II

The disturbance in Case II is the same as that in Case I, and the comparison between the mode-switching strategy and a kind of adaptive droop control method is investigated. The DC voltage deviation-dependent voltage droop control proposed in [26] is revised and adopted in this case, whose control law is expressed as:

$$\beta_{\mathrm{adp}} = \begin{cases} \beta & |\Delta V_{\mathrm{dc}}| \le \delta_{\mathrm{adp-tri}} \\ \beta \frac{|\Delta V_{\mathrm{dc}}|}{\delta_{\mathrm{adp-tri}}} & |\Delta V_{\mathrm{dc}}| > \delta_{\mathrm{adp-tri}} \end{cases} \tag{14}$$

where β_{adp} denotes the DC voltage deviation-dependent droop gain, and $\delta_{\mathrm{adp-tri}}$ denotes the trigger threshold value. In order to achieve the maximum power when the DC voltage deviation hits the safety limit, the following equation should be satisfied.

$$\beta \frac{\delta_{\mathrm{lim}}}{\delta_{\mathrm{adp-tri}}} \delta_{\mathrm{lim}} + (|P_{\mathrm{ref}}| - P_{\mathrm{max}}) = 0 \tag{15}$$

Consequently, the trigger threshold value of the DC voltage deviation-dependent droop control in this case can be set to 3.5%. The simulation results are illustrated in Fig. 10. In addition, the power waveforms of wind farms are the same as Fig. 9(c) and the operation mode state of the mode-switching strategy is identical to Fig. 9(d).

Compared with Figs. 9 and 10, the DC voltage deviation-dependent droop control also alleviates the DC voltage rising, whereas a little excess (1 kV) can be observed at the VSC1 outage. During the transient process, the DC voltage deviation under its regulation is still larger than that of the proposed strategy. Furthermore, since it does not change setpoints, a

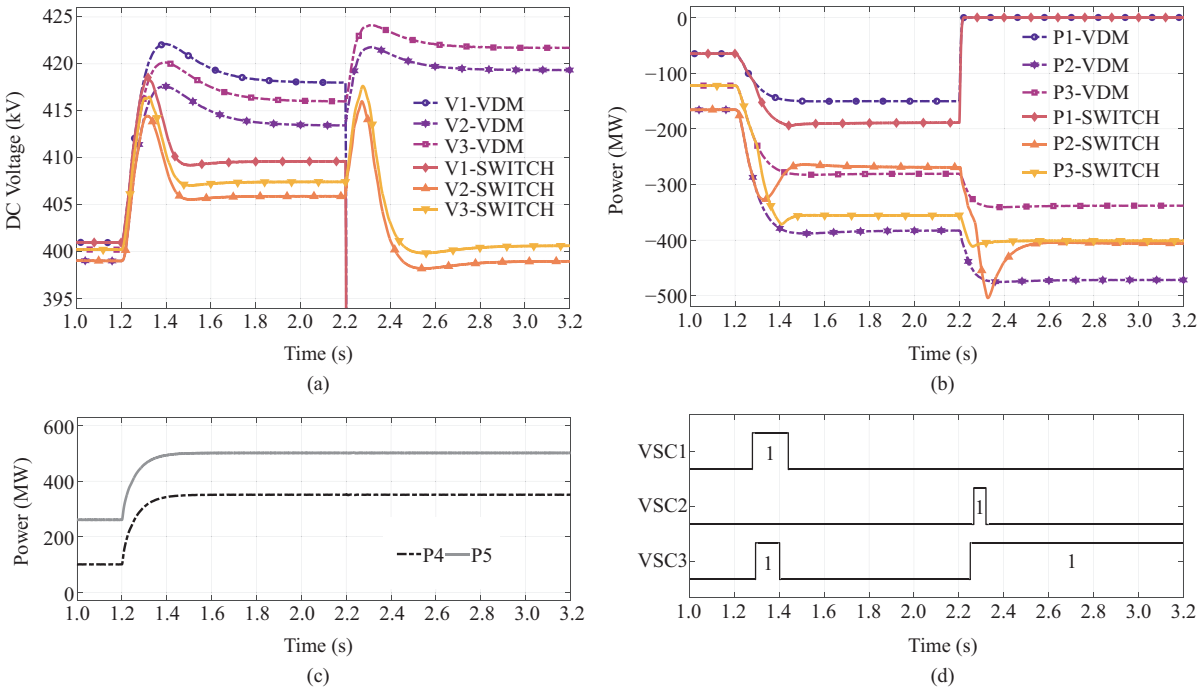

Fig. 9. Simulations of CASE I, where -VDM represents the conventional VDM and -SWITCH represents the mode-switching strategy. (a) DC voltage simulation results, where V1, V2, and V3 denote the dc voltage of VSC1, VSC2, and VSC3. (b) Power simulation results, where P1, P2, and P3 denote the exchanged power of VSC1, VSC2, and VSC3. (c) Exchanged power of VSC4 and VSC5. (d) Mode state of the mode-switching strategy.

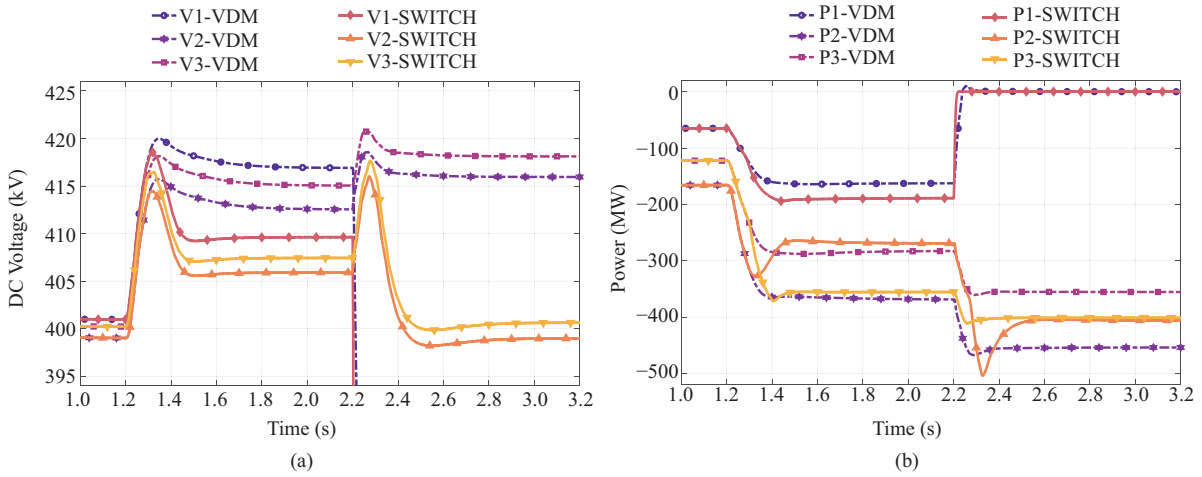

Fig. 10. Simulations of CASE II, where -AVDM represents the dc voltage deviation-dependent droop control and -SWITCH represents the mode-switching strategy. (a) DC voltage simulation results, where V1, V2, and V3 denote the dc voltage of VSC1, VSC2, and VSC3. (b) Power simulation results, where P1, P2, and P3 denote the exchanged power of VSC1, VSC2, and VSC3.

significant DC voltage deviation at steady-state is retained. Meanwhile, owing to the effect of the mode recovery process, better steady-state performance is achieved by the proposed strategy. As depicted in Fig. 10, compared with DC voltage-deviation droop control, despite the DC voltage variation being reduced, the mode-switching strategy realizes a relatively uneven power-sharing.

In summary, it can be said that the mode-switching strategy possesses a better DC voltage regulation capability than the DC voltage deviation-dependent droop control.

C. Case III

The disturbances in Case III are as follows: 1) At 1.2 s, the line disconnection between bus 1 and bus 4 (F2 in Fig. 8) occurs. 2) At 1.6 s, the output power of wind farm1 increases from 100 MW to 350 MW, and the output power of wind farm 2 increases from 260 MW to 500 MW. The simulation results are illustrated in Fig. 11. The second disturbance results in DC voltage rising because the injection power promptly increased.

The complex DC circuit short fault is replaced by the line disconnection realized by DC circuit breakers. When the line disconnection occurs at 1.2 s, DC voltage fluctuations with a minimum value greater than 390 kV can be observed. Therefore, the mode-switching strategy will not be activated. The same dynamic performance of DC voltage and power is realized by both conventional VDM and the proposed strategy.

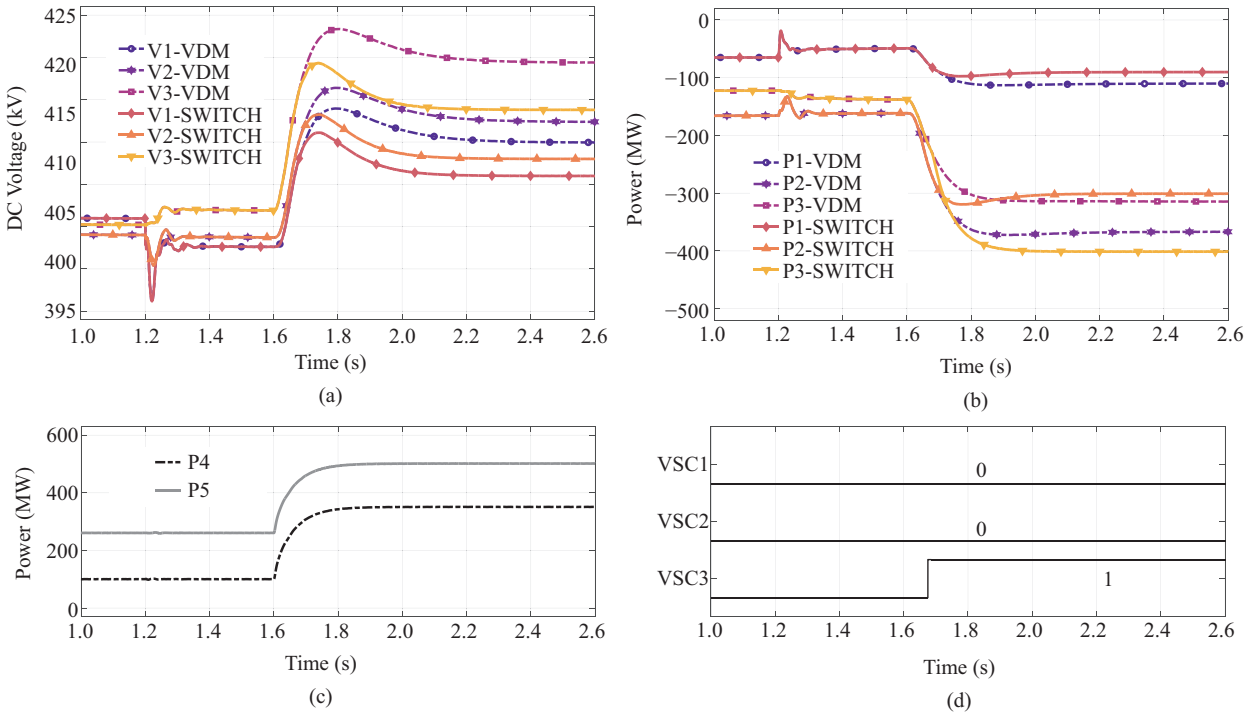

Fig. 11. Simulations of CASE III, where -VDM represents the conventional VDM and -SWITCH represents the mode-switching strategy. (a) DC voltage simulation results, where V1, V2, and V3 denote the dc voltage of VSC1, VSC2, and VSC3. (b) Power simulation results, where P1, P2, and P3 denote the exchanged power of VSC1, VSC2, and VSC3. (c) Exchanged power of VSC4 and VSC5. (d) Mode state of the mode-switching strategy.

After the transient process that lasts approximately 0.2 s caused by the line disconnection, a new steady-state with an open-loop grid structure is achieved. Owing to the certain power flow in the open-loop system, the DC voltage of VSC1 will be the lowest, and the DC voltage of VSC3 will be the highest among the droop-controlled converters.

The increasing output power of wind farms at 1.6 s leads to the DC voltage rising. With the conventional VDM, the DC voltage of VSC3 exceeds its safety limit during the second disturbance, while VSC1 and VSC2 are within the specified range. On the contrary, all the DC voltages of VSC1, VSC2, and VSC3 are below the safety limit under the mode-switching strategy.

The DC voltage of VSC3 reaches the trigger threshold value at 1.675 s, then the mode-switching is activated. The exchanged power of VSC3 immediately increases to 400 MW since its mode is shifted from the voltage droop control to the constant maximum power control. However, because the DC voltage of VSC3 is still greater than the recovery threshold value at the steady-state, its constant maximum power mode remains. The increased power of VSC3 results in a smaller DC voltage deviation and further decreases the power of VSC1 and VSC2. In addition, a smooth power change in VSC3 can also be observed during the mode-switching process.

The comparison between Case I and Case III implies that system topologies affect the operation of the mode-switching strategy, which is nearly inevitable because only the local information has been acquired. However, the proposed strategy is a primary approach to improve the local DC voltage behavior in the short term. The centralized control will be implemented next to further enhance the performance of the VSC-MTDC system. Simulation results have proven the effectiveness of the mode-switching strategy, which exploits the maximum capability of converters to participate in DC voltage regulation.

V. Conclusion

It is elaborated that a close interaction exists between the node injection power and the node DC voltage in the MTDC system. On this foundation, this paper indicates that the most effective approach to regulate the local DC voltage is changing the injection power at that node. According to operating point trajectories of different voltage droop controls with the DC voltage variation, it is determined that switching the operation mode of converters from voltage droop control to constant maximum power control can exert the maximum DC voltage regulation capability. Therefore, a mode-switching strategy is proposed for restricting the transient DC voltage within the specified range in case of disturbances. To regain the capability of converters to maintain DC voltage stable at steady-state and improve system reliability, a mode recovery is developed. It modifies the setpoint while switching the mode from constant maximum power control to voltage droop control. Moreover, the smooth switching method is included for smoothing the power change during the mode switching.

Three cases based on a five-terminal VSC-HVDC system are investigated to validate the mode-switching strategy. Compared with the conventional voltage droop control, simulation results indicate that the proposed strategy effectively alleviates the DC voltage deviation rising during the disturbances and smooths the power during the mode switching process.

Realization of the transient DC voltage below the safety limit and a small DC voltage deviation at steady-state is achieved by the proposed strategy. Furthermore, compared with the DC voltage deviation-dependent droop control, the mode-switching strategy presents a stronger DC voltage regulation capability.

REFERENCES

[1] T. A. Tsalis, K. E. Malamateniou, D. Koulouriotis, and I. E. Nikolaou, "New challenges for corporate sustainability reporting: United Nations' 2030 Agenda for sustainable development and the sustainable development goals," *Corporate Social Responsibility and Environmental Management*, vol. 27, no. 4, pp. 1617–1629, Jul./Aug. 2020.

[2] P. Yan, C. W. Xiao, L. Xu, G. R. Yu, A. Li, S. Piao, and N. P. He, "Biomass energy in China's terrestrial ecosystems: Insights into the nation's sustainable energy supply," *Renewable and Sustainable Energy Reviews*, vol. 127, pp. 109857, Jul. 2020.

[3] M. Wang, T. An, H. Ergun, Y. L. Lan, B. Andersen, M. Szechtman, W. Leterme, J. Beerten, and D. Van Hertem, "Review and outlook of HVDC grids as backbone of transmission system," *CSEE Journal of Power and Energy Systems*, vol. 7, no. 4, pp. 797–810, Jul. 2021.

[4] J. D. Páez, D. Frey, J. Maneiro, S. Bacha, and P. Dworakowski, "Overview of DC–DC converters dedicated to HVdc grids," *IEEE Transactions on Power Delivery*, vol. 34, no. 1, pp. 119–128, Feb. 2019.

[5] P. Bakas, Y. Okazaki, A. Shukla, S. K. Patro, K. Ilves, F. Dijkhuizen, and A. Nami, "Review of hybrid multilevel converter topologies utilizing thyristors for HVDC applications," *IEEE Transactions on Power Electronics*, vol. 36, no. 1, pp. 174–190, Jan. 2021.

[6] A. Alassi, S. Bañales, O. Ellabban, G. Adam, and C. MacIver, "HVDC Transmission: technology review, market trends and future outlook," *Renewable and Sustainable Energy Reviews*, vol. 112, pp. 530–554, Sep. 2019.

[7] Q. Zhao, J. García-González, O. Gomis-Bellmunt, E. Prieto-Araujo, and F. M. Echavarren, "Impact of converter losses on the optimal power flow solution of hybrid networks based on VSC-MTDC," *Electric Power Systems Research*, vol. 151, pp. 395–403, Oct. 2017.

[8] S. L. Gao, Y. Chen, S. W. Huang, and Y. Xia, "Efficient power flow algorithm for AC/MTDC considering complementary constraints of VSC's reactive power and AC node voltage," *IEEE Transactions on Power Systems*, vol. 36, no. 3, pp. 2481–2490, May 2021.

[9] W. N. Zheng, J. B. Hu, and X. M. Yuan, "Modeling of VSCs considering input and output active power dynamics for multi-terminal HVDC interaction analysis in DC voltage control timescale," *IEEE Transactions on Energy Conversion*, vol. 34, no. 4, pp. 2008–2018, Dec. 2019.

[10] P. F. Li, X. L. Li, L. Guo, Z. W. Li, C. Qin, and F. Gao, "Reduced-order modeling and stability analysis of MTDC system under droop control in DC voltage control timescale," in *Proceedings of the 2020 IEEE Power & Energy Society General Meeting (PESGM)*, Montreal, QC, Canada, 2020, pp. 1–5.

[11] X. L. Li, L. Guo, C. Hong, Y. Zhang, Y. W. Li, and C. S. Wang, "Hierarchical control of Multiterminal DC grids for large-scale renewable energy integration," *IEEE Transactions on Sustainable Energy*, vol. 9, no. 3, pp. 1448–1457, Jul. 2018.

[12] H. Q. Xiao, K. Q. Sun, J. P. Pan, L. Xiao, C. Gan, and Y. L. Liu, "Coordinated frequency regulation among asynchronous AC grids with an MTDC system," *International Journal of Electrical Power & Energy Systems*, vol. 126, pp. 106604, Mar. 2021.

[13] M. Mehrabankhomartash, M. Saeedifard, and A. Yazdani, "Adjustable wind farm frequency support through multi-terminal HVDC grids," *IEEE Transactions on Sustainable Energy*, vol. 12, no. 2, pp. 1461–1472, Apr. 2021.

[14] T. K. Vrana, J. Beerten, R. Belmans, and O. B. Fosso, "A classification of DC node voltage control methods for HVDC grids," *Electric Power Systems Research*, vol. 103, pp. 137–144, Oct. 2013.

[15] Y. Z. Wang, W. J. Wen, C. S. Wang, H. T. Liu, X. Zhan, and X. L. Xiao, "Adaptive voltage droop control of multiterminal VSC-HVDC systems for DC voltage deviation and power sharing," *IEEE Transactions on Power Delivery*, vol. 34, no. 1, pp. 169–176, Feb. 2019.

[16] S. S. Sayed and A. M. Massoud, "A generalized approach for design of contingency versatile DC voltage droop control in multi-terminal HVDC networks," *International Journal of Electrical Power & Energy Systems*, vol. 126, pp. 106413, Mar. 2021.

[17] Y. Y. Zhang, X. H. Qu, M. D. Tang, R. Y. Yao, and W. Chen, "Design of Nonlinear Droop Control in DC Microgrid for Desired Voltage Regulation and Current Sharing Accuracy," *IEEE Journal on Emerging and Selected Topics in Circuits and Systems*, vol. 11, no. 1, pp. 168–175, Mar. 2021.

[18] B. Li, Q. Q. Li, Y. Z. Wang, W. J. Wen, B. T. Li, and L. Xu, "A novel method to determine droop coefficients of DC voltage control for VSC-MTDC system," *IEEE Transactions on Power Delivery*, vol. 35, no. 5, pp. 2196–2211, Oct. 2020.

[19] M. N. Ambia, K. Meng, W. D. Xiao, A. Al-Durra, and Z. Y. Dong, "Adaptive droop control of multi-terminal HVDC network for frequency regulation and power sharing," *IEEE Transactions on Power Systems*, vol. 36, no. 1, pp. 566–578, Jan. 2021.

[20] Y. S. Zhang, X. K. Meng, A. M. Shotorbani, and L. W. Wang, "Minimization of AC-DC grid transmission loss and DC voltage deviation using adaptive droop control and improved AC-DC power flow algorithm," *IEEE Transactions on Power Systems*, vol. 36, no. 1, pp. 744–756, Jan. 2021.

[21] Y. S. Zhang, A. M. Shotorbani, L. W. Wang, and W. Li, "Distributed voltage regulation and automatic power sharing in multi-terminal HVDC grids," *IEEE Transactions on Power Systems*, vol. 35, no. 5, pp. 3739–3752, Sep. 2020.

[22] N. R. Chaudhuri and B. Chaudhuri, "Adaptive droop control for effective power sharing in multi-terminal DC (MTDC) Grids," *IEEE Transactions on Power Systems*, vol. 28, no. 1, pp. 21–29, Feb. 2013.

[23] Y. Z. Zhang, J. Ravishankar, J. Fletcher, R. Li, and M. X. Han, "Review of modular multilevel converter based multi-terminal HVDC systems for offshore wind power transmission," *Renewable and Sustainable Energy Reviews*, vol. 61, pp. 572–586, Aug. 2016.

[24] Z. W. Khan, H. Minxiao, C. Kai, L. Yang, and A. u. Rehman, "State of the art DC-DC converter topologies for the multi-terminal DC grid applications: a review," in *2020 IEEE International Conference on Power Electronics, Smart Grid and Renewable Energy (PESGRE2020)*, Cochin, India, 2020, pp. 1–7.

[25] Z. C. Yuan, Y. Z. Wang, Y. Yi, C. S. Wang, Y. M. Zhao, and W. J. Wen, "Fast linear power flow algorithm for the study of steady-state performance of DC grid," *IEEE Transactions on Power Systems*, vol. 34, no. 6, pp. 4240–4248, Nov. 2019.

[26] Y. Z. Wang, B. Li, Z. X. Zhou, Z. G. Chen, W. J. Wen, X. L. Li, and C. S. Wang, "DC voltage deviation-dependent voltage droop control method for VSC-MTDC systems under large disturbances," *IET Renewable Power Generation*, vol. 14, no. 5, pp. 891–896, Apr. 2020.

[27] K. Shinoda, A. Benchaib, J. Dai, and X. Guillaud, "Over- and under-voltage containment reserves for droop-based primary voltage control of MTDC grids," *IEEE Transactions on Power Delivery*, vol. 37, no. 1, pp. 125–135, Feb. 2022.

Yizhen Wang received a B.E.E. degree in Electrical Engineering from Tianjin University, Tianjin, China, in 2010, an M.E.E degree in Electrical Engineering from China Electric Power Research Institute (CEPRI), Beijing, China, in 2013, and a Ph.D. degree in Electrical Engineering from Tsinghua University, Beijing, China, in 2017, respectively. Currently, he is an associated Professor with the School of Electrical Engineering and Automation, Tianjin University, Tianjin, China. His current research interests include power system stability analysis, power system protection, and VSC-HVDC systems.

Fengliang Qiu received a B.S. degree in Electrical Engineering from Tianjin University, Tianjin, China, in 2020. He is currently working toward an M.E.E degree at Tianjin University. His research interests include power system stability analysis, power system protection, and VSC-HVDC systems.

Yirun Ji received a Ph.D. degree in Electrical Engineering from Southeast University, Jiangsu, China, in 2019. Currently, he is an Engineer with the Electric Power Research Institute of State Grid JiBei Electric Power Co. Ltd., China. His current research interests include power system control and HVDC systems.

Zhengguang Chen received a B.E.E. degree in Electrical Engineering from Xi'an Jiaotong University, Shaanxi, China, in 2010, an M.E.E degree in Electrical Engineering from China Electric Power Research Institute (CEPRI), Beijing, China, in 2013. Currently, he is an Engineer with State Grid Corporation of China. His current research interests include power system protection and HVDC systems.

Chengshan Wang received a Ph.D. degree in Electrical Engineering from Tianjin University, Tianjin, China, in 1991. From 1994 to 1996, he was a Senior Academic Visitor with Cornell University, Ithaca, USA. From 2001 to 2002, he was a Visiting Professor with Carnegie Mellon University, Pittsburgh, USA. He is currently a Professor with the School of Electrical Engineering and Automation, Tianjin University, where he is also the Director of the Key Laboratory of Smart Grid of the Ministry of Education. His current research interests include distribution system analysis and planning, distributed generation system and micro-grid, and power system security analysis.